Troy/TNFRSF19 marks epithelial progenitor cells during mouse kidney development that continue to contribute to turnover in adult kidney

Frans Schutgens[a,b], Maarten B. Rookmaaker[b], Francis Blokzijl[c,d], Ruben van Boxtel[c,d], Robert Vries[e], Edwin Cuppen[c,d], Marianne C. Verhaar[b], and Hans Clevers[a,1]

[a]Hubrecht Institute–Royal Netherlands Academy of Arts and Sciences, 3584 CT Utrecht, The Netherlands; [b]Department of Nephrology and Hypertension, University Medical Center Utrecht, 3584 CX Utrecht, The Netherlands; [c]Center for Molecular Medicine, Department of Genetics, University Medical Center Utrecht, 3584 CX Utrecht, The Netherlands; [d]Cancer Genomics Netherlands, University Medical Center Utrecht, 3584 CX Utrecht, The Netherlands; and [e]Hubrecht Organoid Technology, 3584 CM Utrecht, The Netherlands

Contributed by Hans Clevers, November 17, 2017 (sent for review August 22, 2017; reviewed by Jos Joore and Bart Smeets)

During kidney development, progressively committed progenitor cells give rise to the distinct segments of the nephron, the functional unit of the kidney. Similar segment-committed progenitor cells are thought to be involved in the homeostasis of adult kidney. However, markers for most segment-committed progenitor cells remain to be identified. Here, we evaluate *Troy/TNFRSF19* as a segment-committed nephron progenitor cell marker. Troy is expressed in the ureteric bud during embryonic development. During postnatal nephrogenesis, Troy$^+$ cells are present in the cortex and papilla and display an immature tubular phenotype. Tracing of Troy$^+$ cells during nephrogenesis demonstrates that Troy$^+$ cells clonally give rise to tubular structures that persist for up to 2 y after induction. Troy$^+$ cells have a 40-fold higher capacity than Troy$^-$ cells to form organoids, which is considered a stem cell property in vitro. In the adult kidney, Troy$^+$ cells are present in the papilla and these cells continue to contribute to collecting duct formation during homeostasis. The number of Troy-derived cells increases after folic acid-induced injury. Our data show that Troy marks a renal stem/progenitor cell population in the developing kidney that in adult kidney contributes to homeostasis, predominantly of the collecting duct, and regeneration.

kidney | stem cell | development | organoids | lineage tracing

The kidney plays a crucial role in blood pressure regulation, interior milieu homeostasis, and hormone production. The human kidney consists of 1 million nephrons, which are the functional units of the kidney. In mammals, nephrons arise exclusively during embryonic development, and in some species, including mouse, this process is continued during early postnatal development. After nephrogenesis has ceased, a low level of tubular cell turnover persists. However, no new nephrons are formed. The formation of insufficient nephrons during development, commonly referred to as "low nephron endowment," poses a risk for kidney disease in later life (1). Moreover, damage exceeding the capacity of renal tubules to replace injured cells leads to loss of nephrons without replacement. The progressive loss of nephrons is the final common pathway of renal disease. Identification of the mechanisms and progenitor cells involved in renal development as well as adult organ homeostasis provides insights into kidney (patho)physiology and will facilitate the development of new diagnostic and therapeutic strategies.

Historically, research has focused on progenitor cells involved in nephrogenesis during embryonic development. Developmental studies have shown that the kidney is formed by the interaction of two distinct mesodermal cell populations, the ureteric bud (UB), where the self-renewing stem cell population particularly resides in the tips (2, 3), and the metanephric mesenchyme (MM). Upon the interaction between the UB and MM, nephrons are formed in a process that is dependent on Wnt signaling (4). Quickly after the induction of nephron formation, differentiation toward the distinct segments of the nephron, which are all derived from the MM except for the collecting duct (CD) (5), occurs. Indeed, it has been demonstrated using lineage tracing that clonal expansions occur during development that do not cross segment barriers (6), showing that segment-committed progenitor cells exist. In line with this, we demonstrated that one single Lgr5$^+$ segment-committed stem cell is responsible for the expansion of the thick ascending limb of Henle's loop (TAL) in each nephron (7). However, until now, no other segment-committed progenitor cells have been identified in the developing kidney.

More recently, also in adult kidneys, the presence of stem cell populations has been suggested. With elegant lineage tracing experiments, the golden standard for identification of stem cell populations, it has been demonstrated that during adult homeostasis and repair, clonal expansions occur that do not cross segment barriers. This suggests that adult segment-committed progenitor cells exist that clonally expand (6). However, no markers for these segment-committed stem cells have been identified.

In this study, we evaluate the Wnt target gene *Troy* (*TNFRSF19*) as a stem cell marker in the developing and adult kidney. Wnt target genes and proteins are of specific interest for the identification of renal progenitor cells, as Wnt signaling is both essential for kidney

Significance

Chronic kidney disease is a worldwide public health problem on the rise for which no curative treatments are available. Progressive kidney disease can be viewed as an imbalance between renal cell damage and repair. A better understanding of progenitor cells involved in kidney development and replacement of damaged cells in adult homeostasis may identify new therapeutic targets. Here, we describe *Troy* as a marker gene for epithelial progenitor cells. Lineage tracing shows that Troy$^+$ cells contribute to kidney development. Troy$^+$ cells have a high organoid-forming capacity, which is a stem cell characteristic. Tracing of Troy$^+$ cells in adult kidney shows that the cells contribute to kidney homeostasis, predominantly of the collecting duct, and regeneration.

Author contributions: F.S., M.B.R., F.B., R.v.B., R.V., E.C., M.C.V., and H.C. designed research; F.S. and M.B.R. performed research; H.C. contributed new reagents/analytic tools; F.S., M.B.R., F.B., R.v.B., and E.C. analyzed data; and F.S., M.B.R., M.C.V., and H.C. wrote the paper.

Reviewers: J.J., MIMETAS B.V.; and B.S., Radboud University Medical Centre.

Conflict of interest statement: H.C. is holder of several patents related to organoid technology.

Data deposition: The sequence reported in this paper has been deposited in the GenBank database (accession no. ERP019784).

[1]To whom correspondence should be addressed. Email: h.clevers@hubrecht.eu.

This article contains supporting information online at www.pnas.org/lookup/suppl/doi:10.1073/pnas.1714145115/-/DCSupplemental.

development and involved in adult tubular cell turnover (4, 7, 8). In addition, *Troy* has been shown to mark stem/progenitor cells in the stomach and brain (9–11). Here, we document the presence, localization, and identity of Troy$^+$ cells and its progeny in the developing kidney, as well as during normal cell turnover in the adult kidney.

Results

Troy-EGFP$^+$ Cells Are Present in the UB During Embryonic Development and Mark Undifferentiated Cells in the Postnatal Kidney. To document *Troy* expression during embryonic development, we isolated embryonic kidneys from *Troy-Enhanced Green Fluorescent Protein (EGFP)-ires-CreERT2* mice (n = 8). Embryonic kidneys were isolated at 12 d postcoitum (12 dpc), when the UB starts to invade the MM, and were cultured ex vivo for 1, 2, or 6 d (Fig. 1 *A*–*C*). Troy-EGFP expression was observed in the ureteric bud from the moment of isolation and remained present during the culture period. When kidneys were isolated at postnatal day (P) 1 and 2 (n = 6), Troy-EGFP was detected in the outer cortex as well as in the papilla (Fig. 1*D*).

Next, we phenotypically characterized the Troy-EGFP$^+$ cells at P1 and P2 by immunofluorescent staining for nephron segment-specific markers. It showed that the majority of the Troy-EGFP$^+$ cells did not costain with segment-specific differentiated tubular cell markers: megalin (proximal tubule; Fig. 1*E*), Tamm Horsfall Protein (thick ascending limb of Henle's loop; Fig. 1*F*), calbindin (distal tubule; Fig. 1*G*), AQP2 (principal cells of the collecting duct; Fig. 1*H*), and AE1 (α-intercalated cells, collecting duct; Fig. 1*I*). Although most of the Troy-EGFP$^+$ cells did not costain for these differentiation markers, occasionally some double staining for Troy-EGFP$^+$ cells with AQP2 or megalin is observed (Fig. S1).

Thus, most Troy-EGFP$^+$ cells are relatively undifferentiated cells directly postnatally.

Troy-EGFP$^+$ Cells in the Developing Kidney Express UB/Collecting Duct-Specific Genes. To further characterize the Troy-EGFP$^+$ positive cells during renal development, we performed RNA sequencing of Troy-EGFP$^+$ cells isolated from kidneys from early postnatal (P2) *Troy-EGFP-ires-CreERT2* mice (n = 3) to determine the signature transcriptome. Single cells were FAC sorted into three fractions: strongly Troy-EGFP positive (Troy-EGFP^{++}), weakly Troy-EGFP positive (Troy-EGFP$^+$), and Troy-EGFP negative (Troy-EGFP–) populations (Fig. 2*A*). Five to 10 percent of the living cells at P2 were Troy-EGFP^{++} (with these gating settings, 0.5% of the kidney cells from a wild-type mouse were part of the EGFP$^+$ population). We found that *Troy* expression was highest in the Troy-EGFP^{++} population compared with Troy-EGFP$^+$ and Troy-EGFP$^-$, confirming its identity as the endogenous *Troy*$^+$ kidney population (Fig. 2*B*).

From a previously published dataset (12), we extracted lists of genes that are enriched in the UB and a list of genes that are specifically expressed in the MM. We compared these lists, with the genes that are differentially expressed in the Troy^{++} population, compared with the Troy$^-$ population. We found that genes that were enriched in Troy^{++} population were much more likely to be typical UB genes than MM genes. These findings indicate a predominant UB identity of Troy-EGFP^{++} cells, and MM identity for Troy-EGFP$^-$ cells (Fig. 2*C*).

Next, we performed a similar analysis to assess in greater detail the stages of UB development, by comparing our expression data to an additional dataset (13) that we accessed through the Gudmap database. This microarray based dataset includes two time points, embryonic day (E) 11.5 and E15.5 and examines multiple laser-captured compartments. It is of note that this reference dataset did not find large differences in gene expression across compartments (13) and, therefore, it appeared that many compartments were enriched in the Troy-EGFP^{++} population (Fig. 2*D*). However, within the UB-related compartments, Troy-EGFP^{++} cells had highest up-regulation in E15.5 ureteric tip-specific genes,

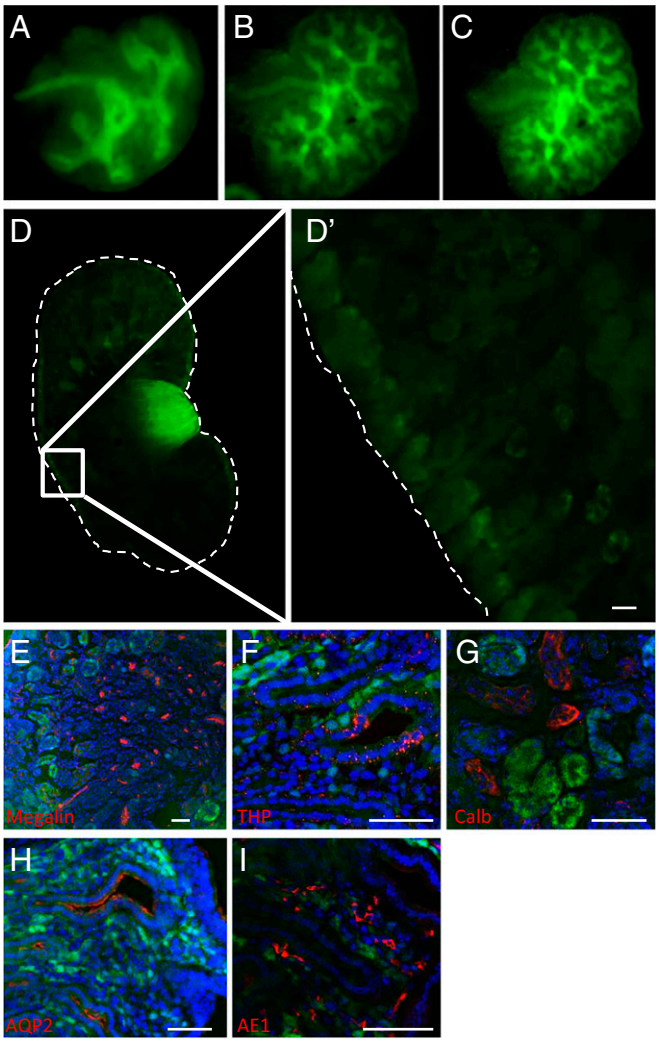

Fig. 1. Troy expression during kidney development. Troy was expressed during embryonic development in the UB at E12.5 (*A*), E13.5 (*B*), and E18.5 (*C*) dpc in ex vivo kidney culture. At P1 and P2, Troy was expressed in the papilla (*D*) and outer cortex (*D* and *D'*). At P2 Troy-EGFP$^+$ cells did not overlap with tubular differentiation markers megalin (*E*), THP (*F*), Calbindin (*G*), AQP2 (*H*), or AE1 (*I*). (*E*–*I*) Visualized with immunofluorescence. (Scale bars: 50 μm.)

showing a ureteric tip identity of Troy-EGFP^{++} cells (Fig. 2*D*). Surprisingly, genes specific to the S-shaped body, a non-UB–related compartment, were also highly up-regulated in the Troy-EGFP^{++} fraction. However, during the S-shaped body stage of kidney development, fusion to the ureteric bud has already taken place, potentially explaining why—at least part of—Troy-EGFP^{++} cells are also enriched for S-shaped body genes. Interestingly, of the compartments in the dataset that remain present in adult kidney (proximal tubule, Loop of Henle, cortical collecting duct, and medullary collecting duct), Troy-EGFP^{++} cells have on average the highest up-regulation in collecting duct-specific genes.

Troy-EGFP$^+$ Cells in the Developing Kidney Exhibit Organoid-Forming Capacity in Vitro. Formation of spheres or organoids in vitro is considered a stem cell capacity (14–16). To assess organoid-forming capacity of Troy-EGFP^{++} cells, we FAC sorted cells derived from P2 kidneys (n = 3 mice) into Troy-EGFP^{++}, Troy-EGFP$^+$, and Troy-EGFP$^-$ populations (Fig. 3*A*) and we seeded 15,000 cells of each fraction in Matrigel as described previously (17). Cells were cultured in culture media supplemented with Wnt3A-, Rspo1-, and

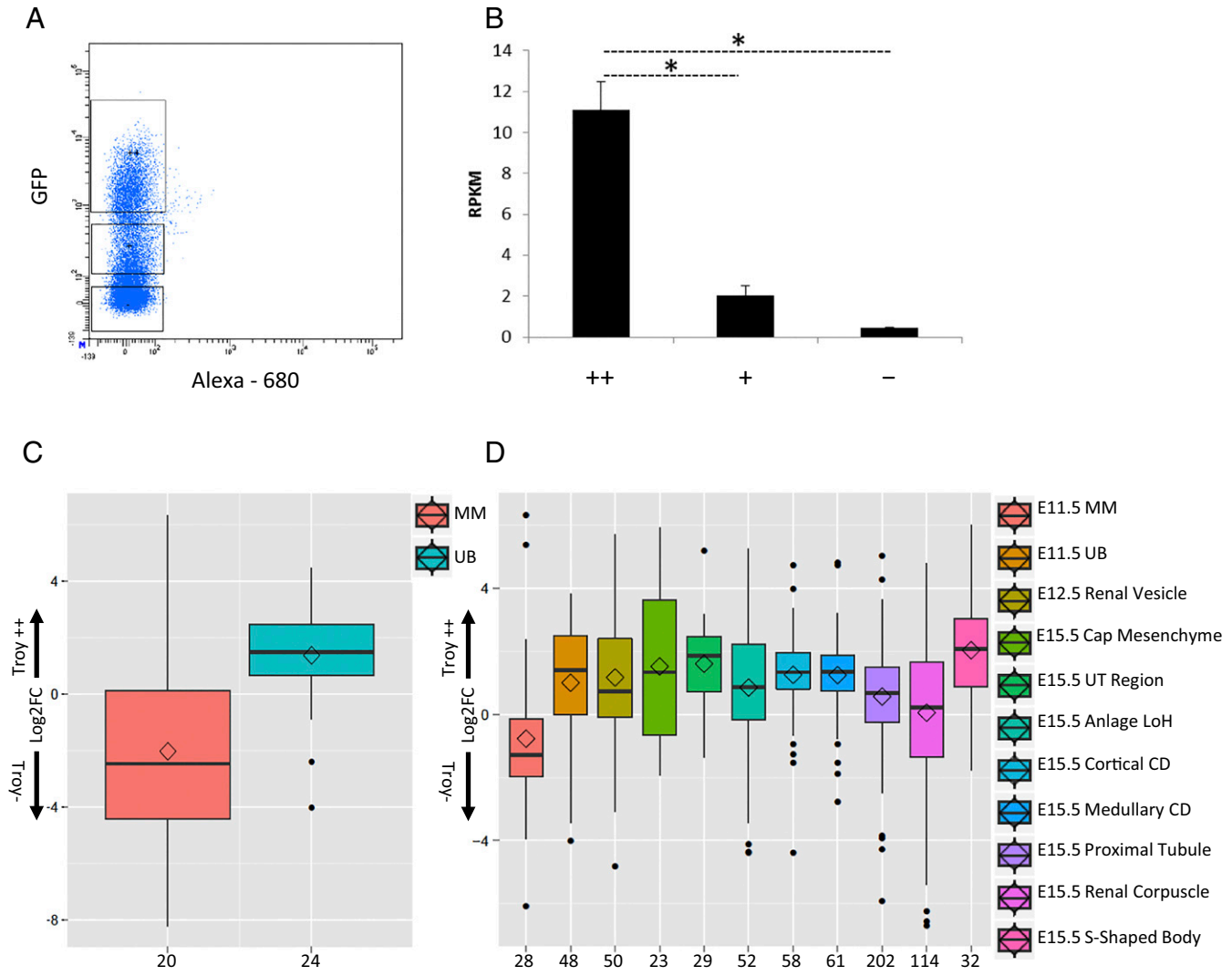

Fig. 2. Transcriptome analysis of P2 Troy-EGFP^{++} versus Troy-EGFP^{-} cells. (*A*) Profile of FAC-sorted Troy-EGFP^{++}, Troy-EGFP^{+}, and Troy-EGFP^{-} cells, from *Troy-EGFP-CreERT2* mice at P2; as additional control for autofluorescence, signal in Alexa Fluor 680 channel was measured. (*B*) EGFP^{++} cells had high Troy expression, compared with EGFP^{+} and EGFP^{-} cells, confirming its identity as the endogenous Troy population. Values depicted as Reads Per Kilobase per Million mapped reads (RPKM). Error bars are SD from two replicates and significance is calculated with a one-way ANOVA, followed by Tukey post hoc test, *$P < 0.01$. (*C*) UB-associated genes were up-regulated in Troy-EGFP^{++} cells, compared with Troy-EGFP^{-} population, and MM-specific genes were down-regulated. The total number of genes in the compartment-specific gene sets are indicated below the graph. Gene sets are from ref. 12. (*D*) Within the UB compartments, up-regulation of E15.5 ureteric tip region-specific (*UT region*) genes in Troy^{++} compared with Troy^{-} cells was largest. Within adult compartments, Troy-EGFP^{++} cells are particularly up-regulated in medullary and cortical collecting duct genes. Compartment-specific gene lists were derived from ref. 13. The number of the genes per compartment is indicated below the graph. Diamonds in the box plots (*C* and *D*) depict the mean with confidence intervals.

Noggin-conditioned medium and addition of B27, *N*-acetylcysteine, EGF, FGF10, and A8301.

Sorted Troy-EGFP^{++} cells clonally proliferated, leading to typical cystic organoids, as previously observed for multiple other organs (16) (Fig. 3 *C* and *D*). After 5 d, by scoring cystic structures as depicted in Fig. 3 *C* and *E*, a 40-fold higher colony-forming efficiency of Troy-EGFP^{++} (2.0%) cells was observed, compared with the Troy-EGFP^{-} cells (0.05%), whereas the Troy-EGFP^{+} population had an intermediate efficiency of 0.87% (Fig. 3*B*). The fact that the Troy-EGFP^{+} population has a lower organoid formation capacity than the Troy-EGFP^{++} population may indicate that the level of Troy expression positively correlates with organoid-forming capacity. In the organoids derived from single Troy-EGFP^{++} cells, both EGFP^{+} positive as well as negative cells were present, suggesting loss of the expression of stem/progenitor cell marker Troy (Fig. 3*E*).

To provide definitive prove that the organoids arose in a clonal fashion, we FAC sorted single Troy-EGFP^{+} cells from the culture of cystic structures (as depicted in Fig. 3 *C* and *E*), directly into Matrigel (i.e., one single cell per well). We found that the same epithelium that formed cystic structures formed complex branching structures with 10% efficiency that subsequently could be expanded and maintained over multiple passages (Fig. 3*F*).

Troy-EGFP^{+} Cells Clonally Expand into Tubular Structures During Renal Development. We used in vivo lineage tracing to determine whether the Troy^{+} populations residing within the developing kidney were functioning as renal stem cells in vivo. *Troy-EGFP-ires-CreERT2; Rosa-LacZ* mice were tamoxifen-induced at P1 and traced for 1 (=day 2), 9, and 29 d as well as 2 y. At day 2 ($n = 2$), LacZ^{+} cells were confined to the cortex, whereas at day 10 ($n = 3$), LacZ^{+} structures started to extend into the medulla (Fig. 4 *A–C*). At day 30 ($n = 3$), LacZ^{+} clones extended into the papilla (Fig. 4 *D–F*). In accordance with the histology, quantification of tracing clones revealed that these clones significantly increased in size

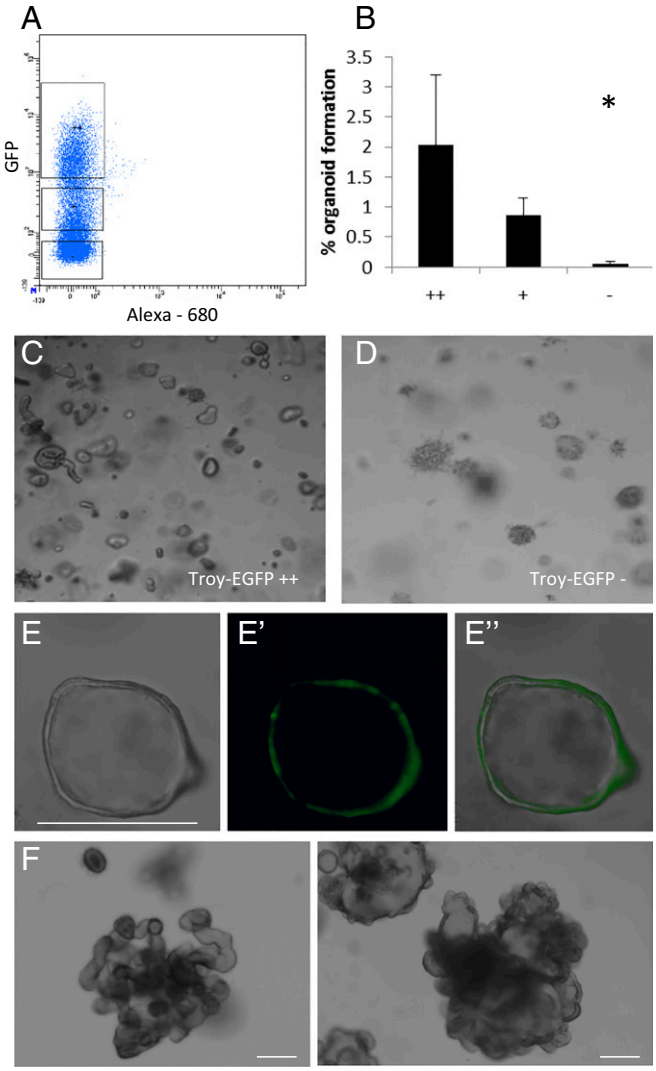

Fig. 3. Troy^{+} cells have organoid-forming capacity. (*A*) Profile of FAC-sorted EGFP populations from P2 kidneys (n = 3) isolated from *Troy-EGFP-ires-CreERT2* mice: Troy^{++} and Troy^{+} were discriminated from the Troy^{-} populations according to their EGFP expression level; as additional control for autofluorescence, signal in Alexa Fluor 680 channel was measured. (*B*) Organoid-forming capacity was significantly ($P < 0.05$) increased in the Troy-EGFP^{++} population compared with the Troy-EGFP^{-} after 5 d. Error bars signify SD. In the Troy-EGFP^{++} cultures, cystic organoids were observed after 5 d (*C*), whereas EGFP^{-} cultures gave rise to mesenchymal-like colonies (*D*). (*E*) The organoids formed in the Troy-EGFP^{++} culture contained both Troy-EGFP^{+} as well as Troy-EGFP^{-} cells. (*F*) To prove that the structures were clonal, we FAC-sorted one single cultured Troy-EGFP^{+} cell per well and complex branching structures formed. Images are from passage 2. (Scale bars: 250 μm.)

over this period of time ($P < 0.01$; Fig. 4*H*). In addition, we observed that these clones not only continuously expand, but that they also persist for at least 2 y after induction (Fig. 4*G*). Of note, homozygous *Troy-EGFP-ires-CreERT2* mice also yielded tracings, indicating that *Troy* is a nonessential stem cell marker.

To identify to which nephron segment Troy-expressing cells gave rise, immunohistochemistry (IHC) for differentiated tubular markers was performed (Fig. 4 *I–L*). IHC revealed that clones predominantly costained for AQP2, a collecting duct marker rather than for markers for the proximal tubule (Fig. 4*J*), loop of Henle (Fig. 4*K*), or distal tubule (Fig. 4*L*). However, particularly in the long-term tracings, costaining also was observed for megalin, THP, and calbindin (Fig. S2).

To assess whether these LacZ^{+} expansions were clonal (and not the result of clustering of multiple independent Troy^{+} cells that together gave rise to a tubular structure), we employed *Troy-GFP-ires-CreERT2; R26R-confetti* mice that after tamoxifen induction randomly express one of four fluorescent proteins (18). Again, mice were induced at P1 and traced for 30 (n = 3), 60 (n = 3), 90 (n = 3), 180 (n = 3), 365 (n = 3), and 540 d (n = 2). Single-colored clones were detected at distinct time points (Fig. 4 *M* and *N*), indicating that one clone arose from one single Troy^{+} cell (otherwise, clones of mixed colors would have been detected). In addition, clones persisted for at least 1.5 y. Fewer clones were observed per induced kidney than in the LacZ tracings (7), in agreement with the lower sensitivity of the *R26R-confetti* allele (18).

Troy-EGFP^{+} Cells Are Present in the Papilla in the Adult Kidney. Next, we assessed the presence of Troy^{+} cells in the kidney after completion of nephrogenesis. In 5-wk-old *Troy-EGFP* mice, the presence of Troy-EGFP^{+} cells was limited to the papilla (Fig. 5*A* and Fig. S3) and Troy expression was more limited in the adult kidney compared with P1 kidney. No costaining was observed with megalin, THP, and calbindin (Fig. S4). Costaining occurred with AE1 (α-intercalated cells of the collecting duct; Fig. 5*B*) and AQP2 (principal cells of the collecting duct; Fig. 5*C*).

Troy-EGFP^{+} Cells Clonally Expand into Tubular Structures During Adult Renal Cell Turnover. We induced *Troy-GFP-ires-CreERT2; Rosa-LacZ* mice with tamoxifen at P35 and followed tracing for up to 1 y (1, 7, 21, 63, 181, 365 d). As expected, the LacZ^{+} cells were present in the papilla only, and the number of LacZ^{+} cells was limited, compared with P1-induced kidney, but the labeled LacZ^{+} structures increased significantly over time (Fig. 5 *D–F*, *J*, and *K*). IHC revealed predominant costaining with AQP2, a marker of principal cells of the collecting duct (Fig. 5*H*) and AE1 (marker of intercalated cells of the collecting duct; Fig. 5*I*).

As the number and size of the LacZ tracing clones was limited, we employed *Troy-GFP-ires-CreERT2; Rosa-tdTomato* mice, with a higher reporter efficiency to confirm our LacZ tracings. We induced at day 56 and found that 14 d after induction, Troy-derived tubular structures were present, predominantly in the papilla (Fig. S5). These structures increased in size over time and remained present on the long term, as assessed after 1 y of tracing (Fig. 5 *L* and *L′*).

Troy-Derived Cells Contribute to Regeneration After Reversible Injury. To further substantiate the findings of Troy^{+} cells as stem/progenitor cell, we assessed whether Troy^{+} cells contributed to regeneration. Injection of folic acid is known to induce injury in both proximal tubule and collecting duct (19). To confirm that folic acid induced tubular damage, histology was assessed. After 7 d, histology revealed signs of tubular kidney injury, including tubular dilation, cast formation and cell shedding [Fig. 6*A* (vehicle) and Fig. 6*A′* (folic acid)]. Ki-67 staining showed an increase in proliferating cells in the folic acid-injected mice, compared with vehicle-injected mice [Fig. 6*B* (vehicle) and Fig. 6*B′* (folic acid)]. To confirm injury, blood urea levels were measured, and these were increased compared with control (Fig. 6*C*).

After injection of folic acid and tamoxifen induction of *Troy-EGFP-ires-CreERT2; Rosa-LacZ* mice, an increase in LacZ^{+} cells was observed in three of six mice, compared with noninjured and solely tamoxifen-induced (n = 2) mice after 7 d (Fig. 6 *D*, *D′*, *E*, *E′*, and *F*). The Troy-derived cells were present in the papilla only.

Discussion

Our data show that *Troy* marks a progenitor cell population during renal development that also contributes to collecting cell turnover in the adult kidney. A progenitor cell phenotype was supported by the absence of staining for differentiated tubule segment markers. To support our in vivo data, an in vitro organoid-forming capacity

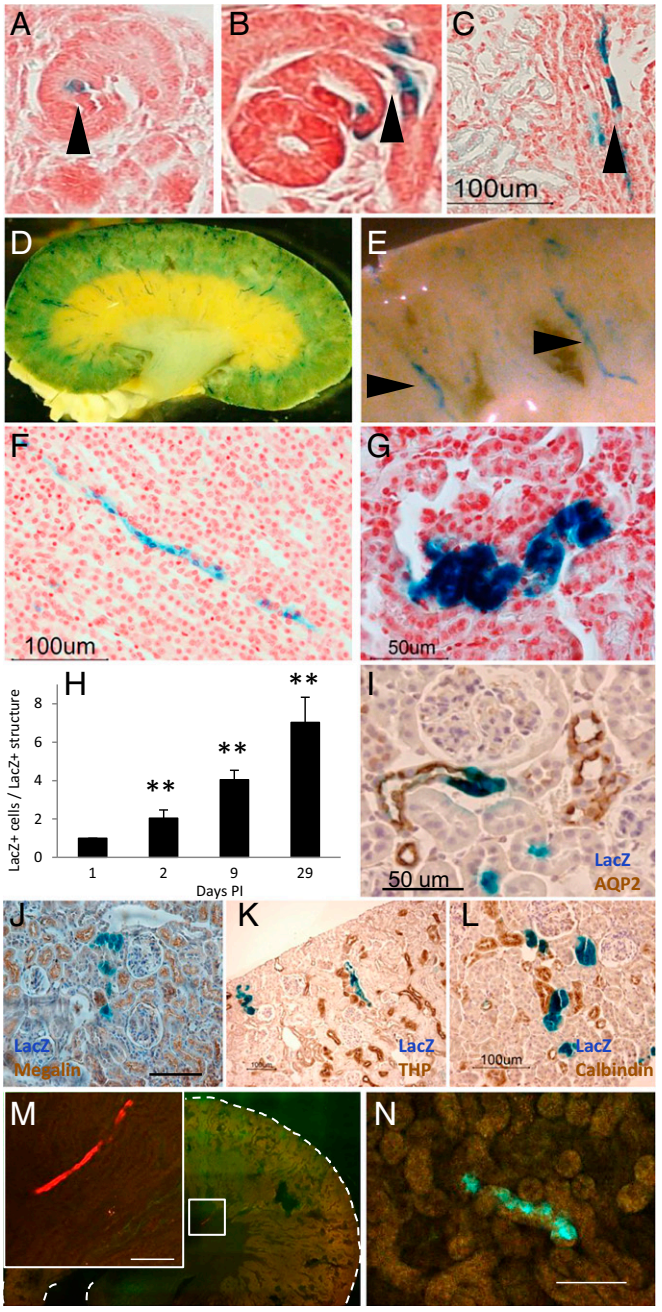

Fig. 4. Troy$^+$ cells formed tubular structures during postnatal kidney development. Kidney sections of P1 induced *Troy-EGFP-ires-CreERT2; Rosa-LacZ* mice, traced for 1 (*A*), 2 (*B*), or 9 d (*C*), indicating the expansion of Troy$^+$ clones (arrowheads). (*D* and *E*) Whole mount images of *Troy-EGFP-ires-CreERT2; Rosa-LacZ* kidneys traced for 29 d and stained for LacZ, indicated that tubular structures (arrowheads) were formed. (*F*) The formation of tubular structures was confirmed with histology on 29 d-traced *Troy-EGFP-ires-CreERT2; Rosa-LacZ* kidney. (*G*) Tubular structures persisted up to 2 y, which was the last time point included in the experiment. (*H*) Quantification of the number of LacZ$^+$ cells per LacZ$^+$ structure shows the significant expansion of LacZ$^+$ clones, as assessed by a one-way ANOVA, followed by a post hoc Tukey test. *P* values of the differences between 1 d after induction vs. different tracing time points are indicated in the graph, $^{**}P < 0.01$. LacZ$^+$ clones costained predominantly with AQP2 (*I*), and not with megalin (*J*), THP (*K*), or calbindin (*L*). (*M* and *N*) Confetti lineage tracing from neonate Troy$^+$ populations revealed the activity of individual Troy$^+$ stem/progenitor cells. Confocal images of the kidneys of P1-induced *Troy-EGFP-ires-CreERT2; R26R-confetti* mice, where a RFP clone that was traced for traced for 1 y (*M*) and a CFP clone that was traced for 90 d (*N*). The single color shows the stem/progenitor outcome of one Troy$^+$ cell. (Scale bars: *C*, *F*, *J*, *M*, and *N*, 100 μm; *G* and *I*, 50 μm.)

was performed that also showed stem cell properties of Troy$^+$ cells. Morphologically, *Troy* appears to be expressed in the UB during embryonic development. At P1, the gene expression profile of the Troy$^+$ cells matched the UB rather than MM, and within the UB, resembled the expression of the ureteric tip region. Moreover, lineage tracing showed that Troy$^+$ cells clonally contributed to distinct nephron segments, including the collecting duct, during postnatal development, as well as collecting duct turnover and regeneration after injury in the adult kidney. Whether this stem/progenitor phenotype of Troy$^+$ cells is hardwired, or rather a state that cells can enter and leave (a "stem cell state"), remains to be identified.

Our findings are in line with other research on renal stem/progenitor cells. Classic recombination experiments have demonstrated that the UB gives rise to the collecting duct, and later others (20) extended this finding and showed that progenitor cell capacity of the early (12 dpc) UB is not restricted to a limited number of UB cells. Accordingly, we note the diffuse Troy expression of the UB in kidneys harvested 12 dpc. More recent experiments demonstrated that self-renewing progenitor cells are predominantly located in the tips of the UB (2, 3, 21), and indeed, we find that Troy^{++} cells have a UB-tip gene signature. Moreover, previous in vivo tracing studies have suggested clonal expansion of single segment-committed stem cells during renal development, homeostasis, and regeneration (6). Our study confirms and extends these findings by providing a marker for a subset of these clonally expanding cells. In addition, our study is complementary to our previous study (7) where we identified Lgr5 as a stem cell marker for the loop of Henle during development. Here, we also elaborate the findings to adult homeostasis and repair. During development, localization of Lgr5 and Troy at E13.5–E14 and P1 is different. Lgr5$^-$ and Troy tracings induced at P1 give macroscopically clones in different regions in the kidney. Thus, although both *Troy* and *Lgr5* are Wnt-target genes, their expression pattern as well as the location and identity of their daughter cells is clearly different. However, there appears to be some overlap in Lgr5 and Troy expression on the RNA level, and P1-induced *Troy* tracings yield some clones that costain with TAL-marker THP (TAL is the predominant phenotype of *Lgr5*-traced cells). A similar situation with different fates for *Troy* and *Lgr5* stem cells exists in the stomach epithelium (11, 22).

We find that the location and relative number of Troy$^+$ cells change during renal development (Fig. 7). During early nephrogenesis (12 dpc), Troy appears to be expressed in almost all UB cells, whereas Troy is expressed in the papilla and outer cortex immediately after birth, when nephrogenesis still takes place. Expression is limited to the papilla when nephrogenesis has ceased 5 wk later. The fact that, although predominantly located at the UB tips, all UB cells have stem cell capacity during early nephrogenesis is in line with previous findings (20) as described above. The cortical localization of perinatal Troy$^+$ stem cells appears to be in line with the notion that nephrogenesis still takes place at the renal cortex at this time point, suggesting the presence of UB stem cells in the cortex. However, at P1, Troy appears to be expressed in progenitor cells of other nephron segments, which is supported by the increased presence of noncollecting duct phenotypes of Troy progeny in the P1-induced tracing experiment and the costaining of Troy cells with noncollecting duct markers like megalin. Localization of progenitor cells in the papilla at P1 and at 5 wk of age extends the findings of the papilla as stem cell niche. The papilla as adult stem cell niche was previously suggested on the basis of DNA label-retaining experiments (23–28).

In the organoid assay of the kidney Troy cells that we used to back up our in vivo data, we found around 2% organoid-forming efficiency, which may appear low for a stem cell. However, similar numbers are observed in intestinal crypt stem cell assays (for instance as described in ref. 29), on which our experiments were based.

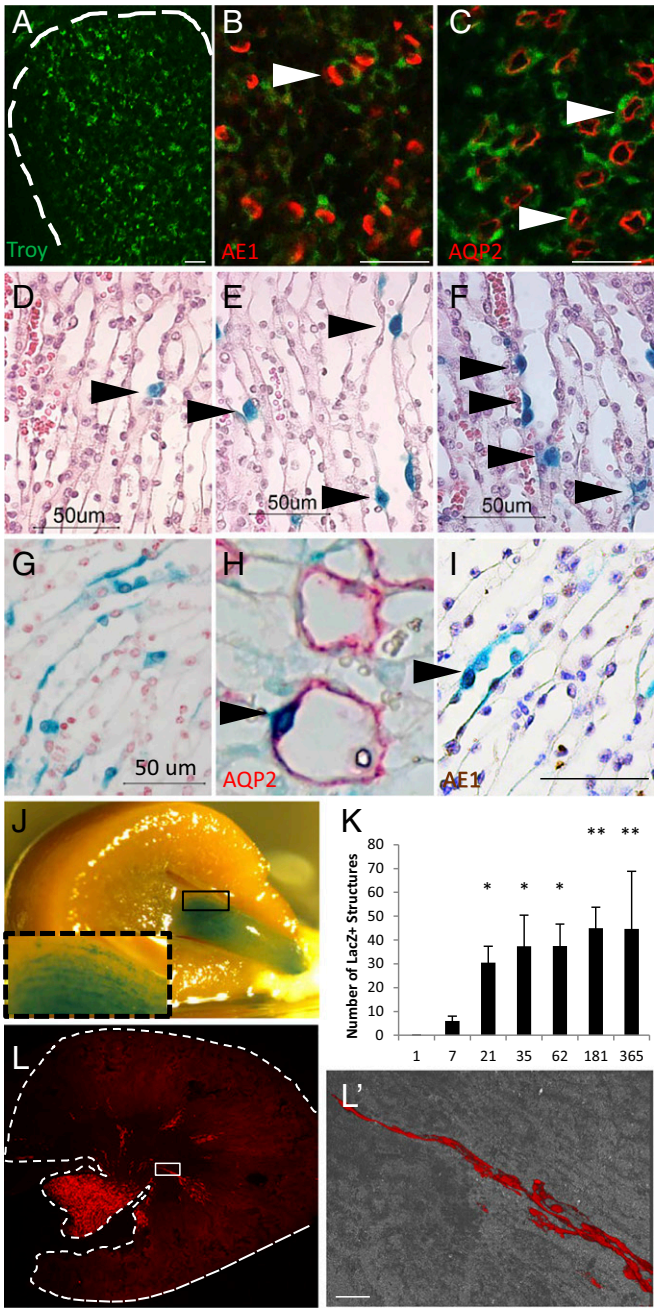

Fig. 5. Troy is expressed in adult kidney and Troy$^+$ cells accumulate over time. (*A*) Troy expression in adult kidney was limited to the papilla, as visualized with confocal imaging. Dashed white line indicates the circumference of the papilla. Costaining (arrowheads) of Troy$^+$ cells with collecting duct markers AE1 (*B*) and AQP2 (*C*), as assessed with immunofluorescence. Sections of *Troy-EGFP-ires-CreERT2* mice show LacZ$^+$ cells (arrowheads) induced at day 35, and traced for 14 (*D*), 30 (*E*), or 90 d (*F*), up to 1 y (*G*). Part of the LacZ$^+$ cells costained with AQP2 (arrowhead) (*H*) and AE1 (arrowhead) (*I*). (*J*) Whole-mount image of an adult kidney traced for 63 d, with detail of the papilla in the dashed box. (*K*) The number of LacZ$^+$ structures per kidney section increases significantly over time. *P* values of the differences between 1 d postinduction vs. different tracing time points are indicated in the graph; $*P < 0.05$, $**P < 0.01$. (*L* and *L*′) Adult-induced (day 56) tracings in *Troy-GFP-ires-CreERT2; Rosa-tdTomato mice,* confocal image of a cross-section, 1 y after induction. *L*′ is a 3D reconstruction from the clone in the white box in *L*. (Scale bars: 50 μm.)

In the intestinal crypt, where epithelial stem cells are understood best, the frequency of Lgr5$^+$ stem cells is in the order of 5–10% of all crypt cells (30). Plating efficiency of these Lgr5 stem cells in purified form is around 1% (29). We have shown that the inefficient plating of crypt stem cells is related to the absence of a real niche cell (29). Importantly, when nonstem cells are plated, the efficiency is 0%. Similarly, kidney stem cells may require neighboring niche cells for essential signals. However, less is known about cell turnover/homeostasis in the kidney than in the intestine and cells potentially providing niche signals have not been identified. Interestingly, for Troy$^+$ cells in the stomach, similar colony-forming percentages are found (5% after 7 d) in previous studies (11).

The relative reduction in number of Troy$^+$ cells in adult kidney compared with the developing kidney can be explained by the increased number of cells per nephron in adult kidney, causing a relative decrease in stem cells. The reduced Troy expression in adult kidneys compared with the developing kidney could also be explained by the low turnover of the kidney during homeostasis (i.e., less cells proliferation of less Troy-EGFP$^+$ cells), which eliminates a requirement for active Troy$^+$ stem cell populations, such as present in the gut (30). Alternatively, stem cells may lose Troy expression, and expression might be induced upon injury. Indeed, we observed an increase in Troy-derived cells after folic acid-induced injury. We did not resolve the mechanism behind this response. It could either be that after injury, Troy expression was induced in a dedicated stem cell, as is observed in the liver (31) and pancreas (32), or it could be that any differentiated cell could enter a (Troy$^+$) stem cell state, which is a mechanism that is also observed in the intestine, where differentiated cells can, when Lgr5$^+$ stem cells are removed, fill the stem cell niche (33). In the proximal tubule of the kidney, it seems that all differentiated epithelial cells have the capacity to dedifferentiate and proliferate (34) and that these cells are not fixed progenitor cells (35). Similarly, in the physiological UB, stem cell capacity is localized to the UB tips (3), but after dissociation (i.e., damage), all UB cells have stem cell capacity (20).

In contrast to the in vivo tracing studies mentioned above, a variety of ex vivo studies have demonstrated differentiation of (mouse and human) adult renal progenitor cells into more than one nephron segment. Rat proximal tubules are in vitro capable of differentiation into structures containing all segments of the nephron, even including the collecting duct (36). A mouse mesenchymal stem cell-like collecting duct progenitor cell population has the in vitro capacity to differentiate into adipocytes and chondrocytes (37), although upon transplantation in vivo, these cells are solely able to contribute to the collecting duct. Multipotent human adult stem cells, marked by CD133 and isolated from cortical kidney tissue, have the in vitro capacity to differentiate into podocytes, endothelial, and epithelial cells (38) or epithelial, osteogenic cells, and adipocytes (39). For obvious reasons, lineage tracings have not been carried out.

Thus, to our knowledge, whenever a lineage tracing or in vivo study is performed, mainly segment-restricted progenitors are found, whereas after in vitro culture, multipotent progenitors are also found, possibly due to nonphysiological transdifferentiation.

In our study, Troy cells give almost exclusively rise to collecting duct cells in the 12 dpc and 5-wk-old mouse kidneys. However, LacZ$^+$ structures from the tracing experiments in P1-induced kidneys also have costaining with megalin, calbindin, and THP, particularly at long-term tracings. One explanation is that these markers display some expression in collecting ducts: Calbindin expression has been observed in collecting duct (40, 41), whereas Kumar et al. (42) observed THP in collecting duct cells. Alternatively, immediately after birth, Troy might also be expressed in progenitor cells for other nephron segments.

To definitively determine the lineage capacity of Troy$^+$ cells, an allele to deplete Troy$^+$ cells and recently developed explant cultures based on primary embryonic renal cells (43, 44) will be of use. The progressive identification of nephron segment-committed stem cells provides fundamental insight in normal

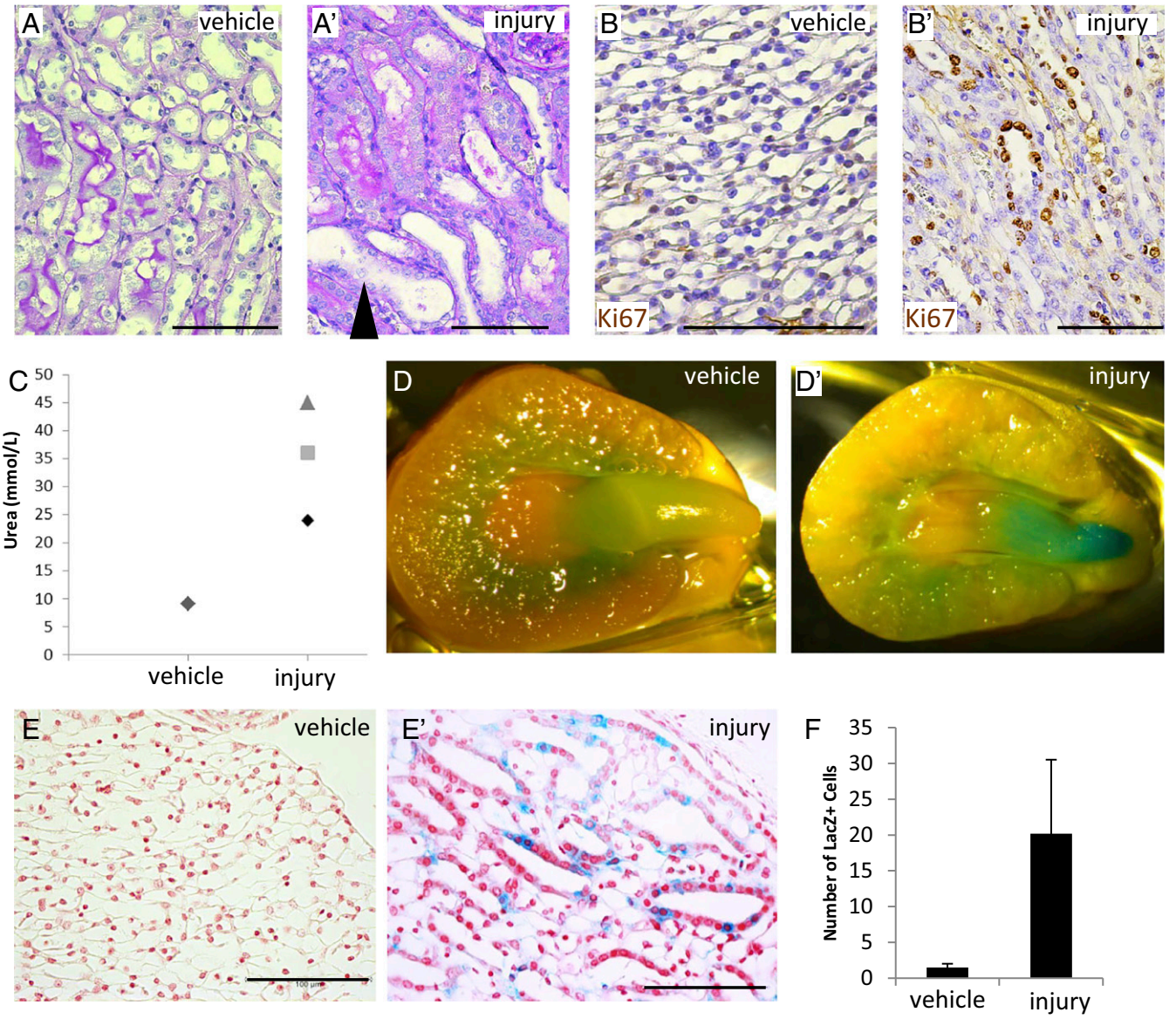

Fig. 6. Troy-derived cells increase after injury induction. (*A*) Histology of a kidney, 7 d after folic acid injection, revealed signs of tubular injury, including tubular dilation, cast formation, and cell shedding (arrowhead), which was not present in the vehicle-treated animals (*A*, vehicle; *A′*, injury). (*B*) Ki-67 staining showed an increase in proliferating cells in the folic acid-injected group compared with vehicle-injected mice (*B*, vehicle; *B′*, injury). (*C*) Folic acid injection led to a significant increase in blood urea levels 1 d after folic acid injection, compared with vehicle injection, indicating kidney injury. (*D*) Whole-mount kidney image from injured and tamoxifen-induced *Troy-EGFP-ires-CreERT2* mice, revealed increased tracings in the papilla after 7 d, compared with a vehicle-injected animal (*D*, vehicle; *D′*, injury). (*E* and *F*) Sections from injured and tamoxifen-induced Troy-EGFP-ires-CreERT2 mice revealed increased tracings after 7 d in the injured animals compared with vehicle-injected animal (*E*, vehicle; *E′*, injury), with the number of $LacZ^+$ cells quantified per kidney section. $n = 2$ vehicle animals; $n = 6$ injury; error bars signify SEM (*F*). (Scale bars: 100 μm.)

physiology and facilitates the evaluation of abnormal development as a first step toward clinical application. Although the relative number of these segment-committed stem cells appears to be low, especially in the adult kidney, previous studies by others (6) and our group (7) suggest that a single segment-committed progenitor is responsible for the formation and homeostasis of that particular nephron segment and, together, the integrity of a whole nephron (5). The ability to determine the number and quality of (committed) progenitor cells (i.e., regenerative capacity) in a renal biopsy may improve its prognostic value. Interestingly, Troy has already been used as a prognostic marker in oncology (45–47). Moreover, the importance of assessing the quality of progenitor cells is highlighted by studies that show that proliferating cells with a prolonged G_2/M cell cycle phase have profibrotic effects leading to chronic kidney disease (48). The fundamental insight in the development and maintenance of nephrons provided by the progressive identification of segment-committed nephron progenitor cells will fuel the development of new diagnostic and therapeutic strategies for renal disease.

Experimental Procedures

Mice. *Troy-EGFP-ires-CreERT2*; *Rosa-lacZ*, *Troy-GFP-ires-CreERT2; Rosa-tdTomato*, and *Troy-EGFP-ires-CreERT2; R26R-confetti* mice were generated (30) as described previously. The Troy knock-in allele was described and validated in the original study (11). *Rosa26RlacZ* mice were obtained from Jackson Labs. All animal experiments were approved by the Animal Experimentation Committee of the Royal Dutch Academy of Science and University Medical Center Utrecht.

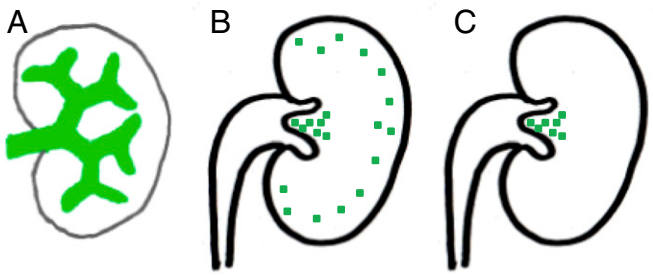

Fig. 7. Localization of Troy expression at different time points. (*A*) Troy is expressed in the ureteric bud during embryonic development. (*B*) Troy is expressed in the nephrogenic zone and in the papilla in the postnatal kidney. (*C*) Troy is expressed in the papilla in the adult kidney during homeostasis and repair.

Tamoxifen Induction. Cre recombinase was activated in *Troy-EGFP-ires-CreERT2*; *Rosa-LacZ* by i.p. injection of 4-hydroxytamoxifen (Sigma). For P1 inductions, a single dose of 10 μL of 4-hydroxytamoxifen in corn oil at 10 mg/mL was used; for P35 inductions, 5 mg of 4-hydroxytamoxifen was injected in a single dose.

With this induction protocol, the contribution of systemically present tamoxifen is limited in three ways. First, induction is done with a single injection of tamoxifen, rather than multiple days in a row. Second, a low dose of tamoxifen is used. Third, 4-hydroxytamoxifen (serum half-life: 6 h; ref. 49) was intraperitoneally injected, rather than tamoxifen (serum half-life: 12 h; ref. 49).

Embryonic ex Vivo Culture. Embryos from timed pregnant mice were isolated 12 d after fertilization using a dissecting microscope (50). Subsequently, they were placed in a Petri dish with cold PBS. Head and tail were removed, the abdominal wall was opened, and intraabdominal organs were removed, by which the retroperitoneum was exposed. The retroperitoneum was carefully removed and kidneys were isolated from it. The embryonic kidneys were placed on a 0.4-μm pore size transwell membrane and cultured at the medium-air interface. Medium [Advanced Dulbecco's modified Eagle's medium (ADMEM)/F12 supplemented with 1% penicillin/streptomycin, Hepes, Glutamax, and 10% FCS] was refreshed every second day. The culture was maintained for 1 wk in a fully humidified 37 °C incubator with 5% CO_2.

β-Galactosidase Staining. To visualize the localization of Troy after tamoxifen induction, kidneys were isolated, halved, and incubated for 2 h in a 20-fold volume of ice-cold fixative [1% formaldehyde, 0.2% glutaraldehyde, 0.02% nonyl phenoxypolyethoxylethanol (Nonidet P-40) in PBS] at 4 °C on a rolling platform. Staining for the presence of β-galactosidase (LacZ) activity was performed as described (22).

Histology and Immunohistochemistry. H&E, PAS, and IHC was performed according to standard protocols on 3- to 4-μm paraffin-embedded sections. The primary antibodies were goat anti-AQP2 (1:200, C-17; Santa Cruz), goat anti-THP (1:500, G-20; Santa Cruz), goat anti-calbindin D28K (1:200, N-18; Santa Cruz), goat anti-megalin (1:200; P-20; Santa Cruz), rabbit anti-AE1 (1:500; Alpha Diagnostics International), and rat-anti-KI67 (1:1,000; eBioscience). All primary antibodies were dissolved in 0.05% BSA in PBS. If required, the secondary antibody rabbit-α-goat-HRP (1:500; Dako) in PBS in 0.05% BSA was used. Goat-α-Rabbit Powervision-Alkaline Phosphatase or Goat-α-Rabbit Powervision-Horse Radish Peroxidase (both Leica Biosystems) were used as secondary or tertiary antibodies, depending on the mode of detection. Staining with Permanent Red (Dako) or Nova Red (Vector laboratories) and counterstained with hematoxylin or light green (Vector Laboratories).

Cryosectioning and Vibratome Sectioning and Confocal Imaging. Isolated kidneys were sliced open and fixed for 30 min (postnatal) or 1 h (adult kidney) in 4% PFA solution at 4 °C. For cryosectioning, kidneys were dehydrated in a 30% sucrose solution in PBS overnight, followed by embedding in tissue freezing medium (Leica) and cryosectioning. For vibratome sectioning, fixed organs were embedded in 4% UltraPure LMP Agarose (Invitrogen) and vibratome sectioned (Leica VT 1000S) at 150 μm as described previously (51). Subsequently, immunofluorescent stainings were carried out with goat anti-AQP2 (1:100, C-17; Santa Cruz), goat anti-THP (1:100, G-20; Santa Cruz), goat anti-calbindin D28K (1:100, N-18; Santa Cruz), goat anti-megalin (1:100; P-20; Santa Cruz), and rabbit anti-AE1 (1:100; Alpha Diagnostics International). Alexa Fluor 568 donkey anti-goat and donkey anti-rabbit IgG were used as secondary antibodies (1:500; Invitrogen).

Then, 150-μm sections were mounted in Hydromount (National Diagnostics) and analyzed for fluorescent protein expression or immunofluorescence by confocal microscopy (Leica SP5).

RNA Sequencing. Kidneys were isolated from neonatal mice (P2). *Troy-EGFP-ires-CreERT2* expressing kidneys were identified by confocal microscopy and this was later confirmed by a genotyping PCR. Kidneys were mechanically disrupted and enzymatically digested with collagenase (C9407; Sigma) and dispase (Invitrogen) and subsequently with TrypLE (Sigma-Aldrich) and DNase. Troy-EGFP^{++}, Troy-EGFP^{+}, and Troy-EGFP^{-} cells (n = 100,000) were sorted by flow cytometry (Moflo; Dako). As additional control for autofluorescence, fluorescence in Alexa Fluor 680 channel was measured. Cells were collected centrifuged and lysed in TriZol reagent (Ambion Life Technologies). Samples from n = 3 mice from two different sorts were pooled and a technical replicate was included.

RNA was extracted using TRIzol (Life Technologies) according to manufacturer's instructions. RNA quality was determined using a Bioanalyser 2100 (Agilent) with an RNA 6000 Nano Kit. Libraries were generated from 100 ng of total RNA using a TruSeq Stranded Total RNA kit with Ribo-zero human/mouse/rat (Illumina no. RS-122-2201) according to manufacturer's instructions. For final application, 15 cycles of PCR were used. Quality of the libraries was determined and libraries were quantified using a Bioanalyser 2100 (Agilent) with a DNA 1000 Kit. Equimolar amounts of libraries were pooled and subjected to single-end, 75-base pair sequencing using an Illumina Nextseq.

RNA Sequencing Analysis. RNA-seq reads were aligned to the mouse reference genome NCBIM37 using STAR (52). The BAM files were sorted with Sambamba v0.5.1 (53), and transcript abundances were quantified with HTSeq-count (54). Subsequently, DESeq 1.16.0 (55) was used to normalize gene counts and to test for differential expression between Troy^{++}, Troy^{+}, and Troy^{-} samples. *P* values were adjusted for multiple testing using Benjamini–Hochberg FDR correction. Adjusted *P* values of <0.05 were considered significantly up- or down-regulated.

To determine which embryonic compartment resembles Troy^{++} cells the most in gene expression, we assessed the differential expression between Troy^{++} and Troy^{-} cells of available compartment-specific gene sets of embryonic mouse kidney (12, 13). Gene symbols were converted to Ensembl Gene ID using org.Mm.eg.db (56), and genes that occurred in multiple segments or genes that we could not link to an Ensembl Gene ID were excluded from the analysis. From ref. 13, genes that were most specific to a compartment (>20-fold up-regulated compared with median expression over all compartments) were included in the analysis.

Organoid Assay. Organoid formation assay is based on the original protocol by Sato et al. (17). Kidneys were isolated and digested into a single-cell suspension and sorted into Troy-EGFP^{++}, Troy-EGFP^{+}, and Troy-EGFP^{-} populations as described under "RNA sequencing." Fifteen thousand cells were resuspended for each condition in growth factor-reduced Matrigel (Corning) and cultured for a week in culture medium (ADMEM/F12 supplemented with 1% penicillin/streptomycin, Hepes, Glutamax), with 1.5% B27 supplement (Gibco), 40% Wnt3a conditioned medium (produced using stably transfected L cells), 10% Noggin conditioned medium, 10% Rspo1-conditioned medium (57), EGF (50 ng/mL; PeproTech), FGF-10 (100 ng/mL; PeproTech), *N*-acetylcysteine (1.25 mM; Sigma) A8301 (5 μM; Tocris Bioscience). Colony-forming capacity was calculated after 5 d of culture.

For the cultures established from a single Troy-EGFP cell, a single-cell suspension from cultured neonatal kidney cells from *Troy-EGFP-ires-CreERT2 mice* was made. Troy-EGFP^{++} cells were sorted (Facsjazz; BD) directly into Matrigel, one Troy-EGFP^{++} cell per well of a 96-well plate. After polymerization of the Matrigel, organoid culture medium was added and organoid cultures (n = 3) were established.

Folic Acid Injury Model. Adult *Troy-EGFP-ires-CreERT2*; *Rosa-lacZ* were subjected to i.p. folic acid injections at 125 mg/mL. One day after injury, Troy expression was induced with tamoxifen as described above. After 7 d, mice were killed for analysis and blood samples were collected for determination of plasma urea (DiaSys Urea CT FS; DiaSysDiagnostic Systems).

Statistical Analysis (Except RNA Sequencing Analysis). Error bars signify mean ± SD, unless otherwise indicated. In case of multiple groups, a one-way ANOVA was performed, combined with Tukey post hoc tests. A *P* value <0.05 is considered statistically significant.

ACKNOWLEDGMENTS. We thank Harry Begthel and Jeroen Korving for preparation of histological and immunohistochemical specimens, Johan van Es and Maaike van den Born for support with the mouse work, the Hubrecht Imaging Center for assistance with (confocal) microscopy, and the Hubrecht FACS facility for help the sort of Troy-EGFP cells. This work was supported by Dutch Kidney Foundation Grant DKF14OP04.

1. Hoy WE, Hughson MD, Bertram JF, Douglas-Denton R, Amann K (2005) Nephron number, hypertension, renal disease, and renal failure. *J Am Soc Nephrol* 16: 2557–2564.
2. Michael L, Davies JA (2004) Pattern and regulation of cell proliferation during murine ureteric bud development. *J Anat* 204:241–255.
3. Shakya R, Watanabe T, Costantini F (2005) The role of GDNF/Ret signaling in ureteric bud cell fate and branching morphogenesis. *Dev Cell* 8:65–74.
4. Carroll TJ, Park J-S, Hayashi S, Majumdar A, McMahon AP (2005) Wnt9b plays a central role in the regulation of mesenchymal to epithelial transitions underlying organogenesis of the mammalian urogenital system. *Dev Cell* 9:283–292.
5. Hendry C, Rumballe B, Moritz K, Little MH (2011) Defining and redefining the nephron progenitor population. *Pediatr Nephrol* 26:1395–1406.
6. Rinkevich Y, et al. (2014) In vivo clonal analysis reveals lineage-restricted progenitor characteristics in mammalian kidney development, maintenance, and regeneration. *Cell Rep* 7:1270–1283.
7. Barker N, et al. (2012) Lgr5(+ve) stem/progenitor cells contribute to nephron formation during kidney development. *Cell Rep* 2:540–552.
8. Kawakami T, Ren S, Duffield JS (2013) Wnt signalling in kidney diseases: Dual roles in renal injury and repair. *J Pathol* 229:221–231.
9. Hisaoka T, Morikawa Y, Kitamura T, Senba E (2004) Expression of a member of tumor necrosis factor receptor superfamily, TROY, in the developing olfactory system. *Glia* 45:313–324.
10. Shao Z, et al. (2005) TAJ/TROY, an orphan TNF receptor family member, binds Nogo-66 receptor 1 and regulates axonal regeneration. *Neuron* 45:353–359.
11. Stange DE, et al. (2013) Differentiated Troy+ chief cells act as reserve stem cells to generate all lineages of the stomach epithelium. *Cell* 155:357–368.
12. Schwab K, et al. (2003) A catalogue of gene expression in the developing kidney. *Kidney Int* 64:1588–1604.
13. Brunskill EW, et al. (2008) Atlas of gene expression in the developing kidney at microanatomic resolution. *Dev Cell* 15:781–791, and erratum (2009) 16:482.
14. Reynolds BA, Weiss S (1996) Clonal and population analyses demonstrate that an EGF-responsive mammalian embryonic CNS precursor is a stem cell. *Dev Biol* 175:1–13.
15. Seaberg RM, et al. (2004) Clonal identification of multipotent precursors from adult mouse pancreas that generate neural and pancreatic lineages. *Nat Biotechnol* 22: 1115–1124.
16. Clevers H (2016) Modeling development and disease with organoids. *Cell* 165: 1586–1597.
17. Sato T, et al. (2009) Single Lgr5 stem cells build crypt-villus structures in vitro without a mesenchymal niche. *Nature* 459:262–265.
18. Snippert HJ, et al. (2010) Intestinal crypt homeostasis results from neutral competition between symmetrically dividing Lgr5 stem cells. *Cell* 143:134–144.
19. Fang T-C, et al. (2005) Proliferation of bone marrow-derived cells contributes to regeneration after folic acid-induced acute tubular injury. *J Am Soc Nephrol* 16: 1723–1732.
20. Unbekandt M, Davies JA (2010) Dissociation of embryonic kidneys followed by reaggregation allows the formation of renal tissues. *Kidney Int* 77:407–416.
21. Riccio P, Cebrian C, Zong H, Hippenmeyer S, Costantini F (2016) *Ret* and *Etv4* promote directed movements of progenitor cells during renal branching morphogenesis. *PLoS Biol* 14:e1002382, and erratum (2016) 14:e1002488.
22. Barker N, et al. (2010) Lgr5(+ve) stem cells drive self-renewal in the stomach and build long-lived gastric units in vitro. *Cell Stem Cell* 6:25–36.
23. Lin S-L, et al. (2010) Macrophage Wnt7b is critical for kidney repair and regeneration. *Proc Natl Acad Sci USA* 107:4194–4199.
24. Whitehouse T, Stotz M, Taylor V, Stidwill R, Singer M (2006) Tissue oxygen and hemodynamics in renal medulla, cortex, and corticomedullary junction during hemorrhage-reperfusion. *Am J Physiol Renal Physiol* 291:F647–F653.
25. Mohyeldin A, Garzón-Muvdi T, Quiñones-Hinojosa A (2010) Oxygen in stem cell biology: A critical component of the stem cell niche. *Cell Stem Cell* 7:150–161.
26. Oliver JA, Maarouf O, Cheema FH, Martens TP, Al-Awqati Q (2004) The renal papilla is a niche for adult kidney stem cells. *J Clin Invest* 114:795–804.
27. Oliver JA, et al. (2009) Proliferation and migration of label-retaining cells of the kidney papilla. *J Am Soc Nephrol* 20:2315–2327.
28. Al-Awqati Q, Oliver JA (2006) The kidney papilla is a stem cells niche. *Stem Cell Rev* 2: 181–184.
29. Sato T, et al. (2011) Paneth cells constitute the niche for Lgr5 stem cells in intestinal crypts. *Nature* 469:415–418.
30. Barker N, et al. (2007) Identification of stem cells in small intestine and colon by marker gene Lgr5. *Nature* 449:1003–1007.
31. Huch M, et al. (2013) In vitro expansion of single Lgr5+ liver stem cells induced by Wnt-driven regeneration. *Nature* 494:247–250.
32. Huch M, et al. (2013) Unlimited in vitro expansion of adult bi-potent pancreas progenitors through the Lgr5/R-spondin axis. *EMBO J* 32:2708–2721.
33. Tetteh PW, et al. (2016) Replacement of lost Lgr5-positive stem cells through plasticity of their enterocyte-lineage daughters. *Cell Stem Cell* 18:203–213.
34. Kusaba T, Lalli M, Kramann R, Kobayashi A, Humphreys BD (2014) Differentiated kidney epithelial cells repair injured proximal tubule. *Proc Natl Acad Sci USA* 111: 1527–1532.
35. Berger K, et al. (2014) Origin of regenerating tubular cells after acute kidney injury. *Proc Natl Acad Sci USA* 111:1533–1538.
36. Kitamura S, Sakurai H, Makino H (2014) Single adult kidney stem/progenitor cells reconstitute 3-dimensional nephron structures in vitro. *Stem Cells* 33:774–784.
37. Li J, et al. (2015) Collecting duct-derived cells display mesenchymal stem cell properties and retain selective in vitro and in vivo epithelial capacity. *J Am Soc Nephrol* 26: 81–94.
38. Bombelli S, et al. (2013) PKH(high) cells within clonal human nephrospheres provide a purified adult renal stem cell population. *Stem Cell Res (Amst)* 11:1163–1177.
39. Sagrinati C, et al. (2006) Isolation and characterization of multipotent progenitor cells from the Bowman's capsule of adult human kidneys. *J Am Soc Nephrol* 17: 2443–2456.
40. Kumar R, Schaefer J, Grande JP, Roche PC (1994) Immunolocalization of calcitriol receptor, 24-hydroxylase cytochrome P-450, and calbindin D28k in human kidney. *Am J Physiol* 266:F477–F485.
41. Davies J (1994) Control of calbindin-D28K expression in developing mouse kidney. *Dev Dyn* 199:45–51.
42. Kumar S, Jasani B, Hunt JS, Moffat DB, Asscher AW (1985) A system for accurate immunolocalization of Tamm-Horsfall protein in renal biopsies. *Histochem J* 17: 1251–1258.
43. Junttila S, et al. (2015) Functional genetic targeting of embryonic kidney progenitor cells ex vivo. *J Am Soc Nephrol* 26:1126–1137.
44. Halt KJ, et al. (2016) CD146(+) cells are essential for kidney vasculature development. *Kidney Int* 90:311–324.
45. Spanjaard RA, Whren KM, Graves C, Bhawan J (2007) Tumor necrosis factor receptor superfamily member TROY is a novel melanoma biomarker and potential therapeutic target. *Int J Cancer* 120:1304–1310.
46. Paulino VM, et al. (2010) TROY (TNFRSF19) is overexpressed in advanced glial tumors and promotes glioblastoma cell invasion via Pyk2-Rac1 signaling. *Mol Cancer Res* 8: 1558–1567.
47. Loftus JC, et al. (2013) TROY (TNFRSF19) promotes glioblastoma survival signaling and therapeutic resistance. *Mol Cancer Res* 11:865–874.
48. Canaud G, Bonventre JV (2015) Cell cycle arrest and the evolution of chronic kidney disease from acute kidney injury. *Nephrol Dial Transplant* 30:575–583.
49. Robinson SP, Langan-Fahey SM, Johnson DA, Jordan VC (1991) Metabolites, pharmacodynamics, and pharmacokinetics of tamoxifen in rats and mice compared to the breast cancer patient. *Drug Metab Dispos* 19:36–43.
50. Giuliani S, et al. (2008) Ex vivo whole embryonic kidney culture: A novel method for research in development, regeneration and transplantation. *J Urol* 179:365–370.
51. Snippert HJ, Schepers AG, Delconte G, Siersema PD, Clevers H (2011) Slide preparation for single-cell-resolution imaging of fluorescent proteins in their three-dimensional near-native environment. *Nat Protoc* 6:1221–1228.
52. Dobin A, et al. (2013) STAR: Ultrafast universal RNA-seq aligner. *Bioinformatics* 29: 15–21.
53. Tarasov A, Vilella AJ, Cuppen E, Nijman IJ, Prins P (2015) Sambamba: Fast processing of NGS alignment formats. *Bioinformatics* 31:2032–2034.
54. Anders S, Pyl PT, Huber W (2014) HTSeq—A Python framework to work with high-throughput sequencing data. *Bioinformatics* 31:166–169.
55. Anders S, Huber W (2010) Differential expression analysis for sequence count data. *Genome Biol* 11:R106.
56. Carlson M (2016) org.Mm.eg.db: Genome wide annotation for Mouse. R package version 2.10.1. Available at dx.doi.org/10.18129/B9.bioc.org.Mm.eg.db. Accessed January 30, 2014.
57. Kim K-A, et al. (2005) Mitogenic influence of human R-spondin1 on the intestinal epithelium. *Science* 309:1256–1259.